

Enhanced and homogeneous oxygen availability during incubation of microfluidic droplets

Lisa Mahler^{a,d,‡}, Miguel Tovar^{a,d,‡}, Thomas Weber^a, Susanne Brandes^{b,d}, Martin Michael Rudolph^a, Josef Ehgartner^c, Torsten Mayr^c, Marc Thilo Figge^{b,d}, Martin Roth^{a,*}, Emerson Zang^{a,*}

Affiliations:

^aBio Pilot Plant and ^bApplied System Biology, Leibniz Institute for Natural Product Research and Infection Biology, Hans Knöll Institute, 07745 Jena, Germany; ^cInstitute of Analytical Chemistry and Food Chemistry, Graz University of Technology, 8010 Graz, Austria; and ^dFaculty of Biology and Pharmacy, Friedrich Schiller University 07743 Jena, Germany

SUPPLEMENTARY INFORMATION

Handling and cultivation of microorganisms	2
Preparation of bacterial cells and spores	2
Single cell encapsulation in droplets	4
Estimation of oxygen depletion time in a droplet.....	4
Calibration of OXNANO sensors	5
Droplet manipulation and analysis.....	7
Microfluidic operation.....	7
Optical setup	8
Volume determination	8
Determination of cell density.....	11
Fluorescence analysis.....	12
Expression analysis of camelid antibody B10-6H	12
Estimation of Oxygen Transfer Rates (OTR) during dynamic droplet incubation	14
Comparison of dynamic droplet incubation with emulsion shaking.....	15
Movie S1.....	20
References.....	21

Handling and cultivation of microorganisms

Preparation of bacterial cells and spores

Bacterial cells, spores and yeast cells were stored at -20 °C as cryo stocks containing 50% of glycerol preservation medium.¹ Before each experiment, bacteria and yeast stocks were diluted in appropriate medium (Tables S2 and S3) and grown for 16-18 h in shaking flasks at 28 °C and 160 rpm. Afterwards, fresh medium was inoculated from the precultures and incubated at 28 °C and 160 rpm until reaching mid exponential phase. Before droplet generation, cell suspensions were diluted in appropriate medium to the indicated optical density and IPTG was added, if required (Table S3). *S. aureofaciens* spore stocks were thawed, diluted in glucose soy peptone (GSP) medium and directly used for droplet generation. Selection antibiotics, when needed (Table S3), were added to precultures only. For comparative experiments between 96-well-plate, shaking flask and droplets, the same cell suspension from a diluted preculture was used for all devices. 50 mL of the cell suspension were incubated at 160 rpm (10 cm shaking diameter) and 28 °C in an unbaffled 500 mL Erlenmeyer shake flask sealed with cotton wool. 200 µL cell suspension were used per microtiter plate (MTP) well. The plates were covered with a breathable seal (AeraSeal®, Excel Scientific, USA) to minimize evaporation and were incubated in an MTP shaker (Shaker DTS-2, neoLab, Germany) at 800 rpm and 28 °C. Droplets were prepared from ~1000 µL of the cell suspension and guided into the incubation devices (Fig. 1 and S1), which were placed with all required periphery at 28 °C.

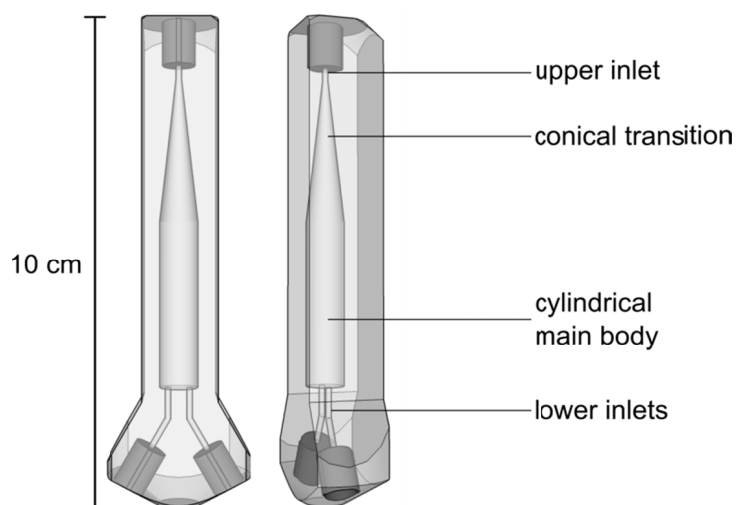


Fig. S1. Front and side view of the droplet incubation device.

Table S1. Culture media. Glucose, thiamine and trace element solution were filter sterilized and added after heat sterilization of all other components.

Medium	Composition
TB	1.2% (w/v) tryptone (Bacto Tryptone, BD Bioscience, Belgium), 2.4% (w/v) yeast extract (Bacto Yeast Extract, BD Bioscience, Belgium), 0.4% (v/v) glycerol (Roth, Germany), 0.17 M KH ₂ PO ₄ (Merck, Germany) and 0.72 M K ₂ HPO ₄ (Merck, Germany) in tap water. pH adjusted to 7.2 with NaOH.
YEPD	1% (w/v) yeast extract (Bacto Yeast Extract, BD Bioscience, Belgium), 2% (w/v) peptone (Bacto Peptone, BD Bioscience, Belgium), and 2% (w/v) glucose (VWR International, USA) in distilled water. pH was adjusted to 6.5 with HCl.
GSP	1% (w/v) soy peptone (Bacto Soytone, BD Bioscience, Belgium), 0.5% (w/v) glucose (VWR International, USA), 85 mM NaCl (Merck, Germany), 0.37 mM KH ₂ PO ₄ (Merck, Germany) and 1 mL/L trace salts solution according to Okanishi ² in deionized water. pH was adjusted to 7.2 with NaOH
M9	44 mM Na ₂ HPO ₄ (Roth, Germany), 22.1 mM KH ₂ PO ₄ (Merck, Germany), 8.56 mM NaCl (Roth, Germany), 18.7 mM NH ₄ Cl (Merck, Germany), 36 μM Zn(CH ₃ COO) ₂ (Merck, Germany), 0.23 mM iron(III) citrate (Fluka, USA), 22.6 μM EDTA (Roth, Germany), 10.5 μM CoCl ₂ (Merck, Germany), 7.6 μM MnCl ₂ (Fluka, USA), 8.8 μM CuCl ₂ (Merck, Germany), 49 μM H ₃ BO ₃ (Merck, Germany), 10.3 μM Na ₂ MoO ₄ (Merck, Germany), 5 mM MgSO ₄ (Merck, Germany), 1% (w/v) glucose (Fluka, USA) and 0.03 mM thiamine (Sigma, USA) in distilled water.

Table S2. Microbial strains, respective media, selection antibiotics, inducers and inoculation densities.

Species	Strain	Medium	Selection marker	Optical density λ = 600 nm	Inducer
<i>Escherichia coli</i>	ECJW992 ^a	TB	ampicillin (100 μg/mL)	1	IPTG (0.5 mM)
<i>Bacillus subtilis</i>	BSNS332-lacI ^b	TB	kanamycin (50 μg/mL)	1	
<i>Pseudomonas fluorescens</i>	IMET10619	TB		1	
<i>Pichia pastoris</i>	M1068	YEPD		1	
<i>Streptomyces aureofaciens</i>	STH449	GSP		5 spores/100 pL	
<i>E. coli</i>	RV308 (p41-B10-6H)	M9	ampicillin (100 μg/mL)	0.5	IPTG (1 mM)

^a*E. coli* JW1982 [origin: Keio collection]³ carrying the pMPAG6 plasmid with *mCherry* cloned downstream of the IPTG-inducible promoter P_{T5}.

^b*B. subtilis* 1s34 carrying the pDG148 plasmid⁴ with *mCherry* cloned downstream of the promoter P_{spac}.

Single cell encapsulation in droplets

The cell concentration was determined and adjusted immediately before starting droplet generation using a Thoma cell counting chamber. Successful single cell encapsulation was confirmed by estimating the proportion of empty versus occupied droplets. According to Poisson's distribution theory, 68% of all droplets are expected to be occupied if an inoculation density of 1 cell/droplet is targeted. It was confirmed after incubation, that this value was neither exceeded for the statically incubated droplets (60.58% occupied) nor for the dynamically incubated droplets (51.41% occupied).

Estimation of oxygen depletion time in a droplet

A conservative estimation of oxygen depletion in statically incubated droplets with encapsulated *E. coli* as a model organism was made on the basis of following simplified assumptions:

1. The net mass transfer across the droplet borders is zero.
2. Oxygen is homogeneously consumed within a droplet, i.e. local depletion in proximity to cells is neglected.

Given (1) $OUR(dt) = OUR_{cell} \cdot N(dt)$

where OUR = oxygen uptake rate [mol/L/h] and OUR_{cell} = oxygen uptake rate per cell [mol/cell/h] and N = number of cells in solution [cell/L] defined as

$$(2) \quad N_t = N_0 \cdot e^{\frac{\ln 2}{t_d} t}$$

where N_0 = starting cell concentration [cells/L] and t_d = doubling time [h], approximate values for the dissolved oxygen depletion times were calculated with relevant parameters extracted from literature or own observations, as listed in table S3. A doubling time of 30 min was assumed for calculation of population size over time.

Table S3. Parameters used for calculation of oxygen depletion time during static droplet incubation. All numbers refer to *E. coli* as a model organism.

Cell concentration at $OD_{600} = 1$	1.2×10^{12} CFU/L (own observation)
Dry cell weight (DCW)	2.78×10^{-16} kg/cell ⁵
Oxygen solubility in complex medium	~0.2 mmol/L
Oxygen uptake rate	0.9-23.1 mol/kg _{DCW} /h ⁶

Assuming an intermediate oxygen consumption rate within the specified range (10 mol/kg/h) and an inoculation density of one cell per 170-pL-droplet, oxygen would be theoretically depleted within ~124 minutes, very similar to the observed 110 minutes in our studies. The usage of smaller droplets translates into a higher cell concentration, which implies faster deoxygenation. For example, in a 14-pL-droplet inoculated with a single cell,⁷ - corresponding to OD₆₀₀ = 0.06 - oxygen should be theoretically depleted within ~38 minutes. Yet, incubation times often exceed this value by far to obtain relevant protein concentrations, so that cells experience hypoxic conditions. At higher inoculation densities (e.g. OD₆₀₀ = 1), eventually achieved by reducing the droplet volume while maintaining Poisson-distributed single-cell occupation, oxygen is theoretically depleted within less than six minutes. Presumably, local oxygen depletion in closest proximity to the cell will further reduce the time until depletion.

Calibration of OXNANO sensors

The OXNANO sensors were calibrated in a temperature controlled glass vessel. Two mass flow controller instruments (Read Y smart series, Vögtlin Instruments) were used to obtain gas mixtures of defined oxygen partial pressures (pO₂). Compressed air and nitrogen were used as calibration gases. The calibration gas was passed through a stainless steel coil which was dipped into a temperature-controlled water bath to keep the temperature constant and bubbled through the OXNANO sensor solution.

The two-site model was used to fit the calibration data.⁸

$$(3) \quad \frac{I_0}{I} = \frac{\tau_0}{\tau} = \left(\frac{f_1}{1+K_{SV,1} \cdot pO_2} + \frac{f_2}{1+K_{SV,2} \cdot pO_2} \right)^{-1}$$

The ratio I_0/I in the model was replaced by τ_0/τ where τ is the lifetime of the oxygen indicator dye at a certain pO₂-value. The lifetime τ_0 represents the lifetime under deoxygenated conditions, where the oxygen indicator is in its unquenched state. The lifetimes were calculated from the phase shift $\Delta\varphi$

recorded by the oxygen meter according to the equation $\tau = \tan(\Delta\phi)/(2\pi f)$, where f is the modulation frequency. The parameters $K_{SV,1}$ ($16.9 \cdot 10^{-3} \text{ hPa}^{-1}$) and $K_{SV,2}$ ($2.05 \cdot 10^{-3} \text{ hPa}^{-1}$) describe the quenching efficiency and thus the sensitivity of the sensor, while the parameters f_1 (0.777) and f_2 characterize different fractions of dye molecules. The dye molecules in fraction f_1 are quenched at $K_{SV,1}$ and molecules in fraction f_2 ($f_2 = 1 - f_1$) are quenched at $K_{SV,2}$. The calibration parameters are shown in table S3.

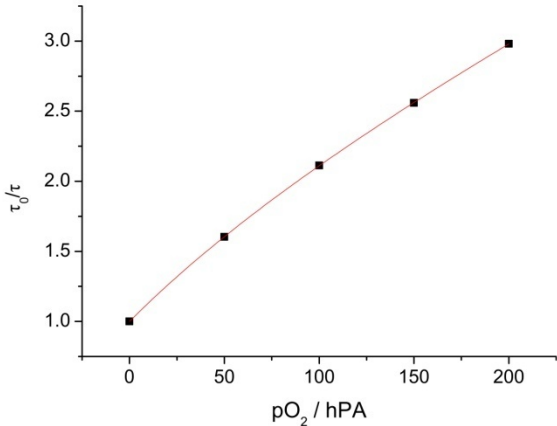


Fig. S2. OXNANO sensors calibration curve.

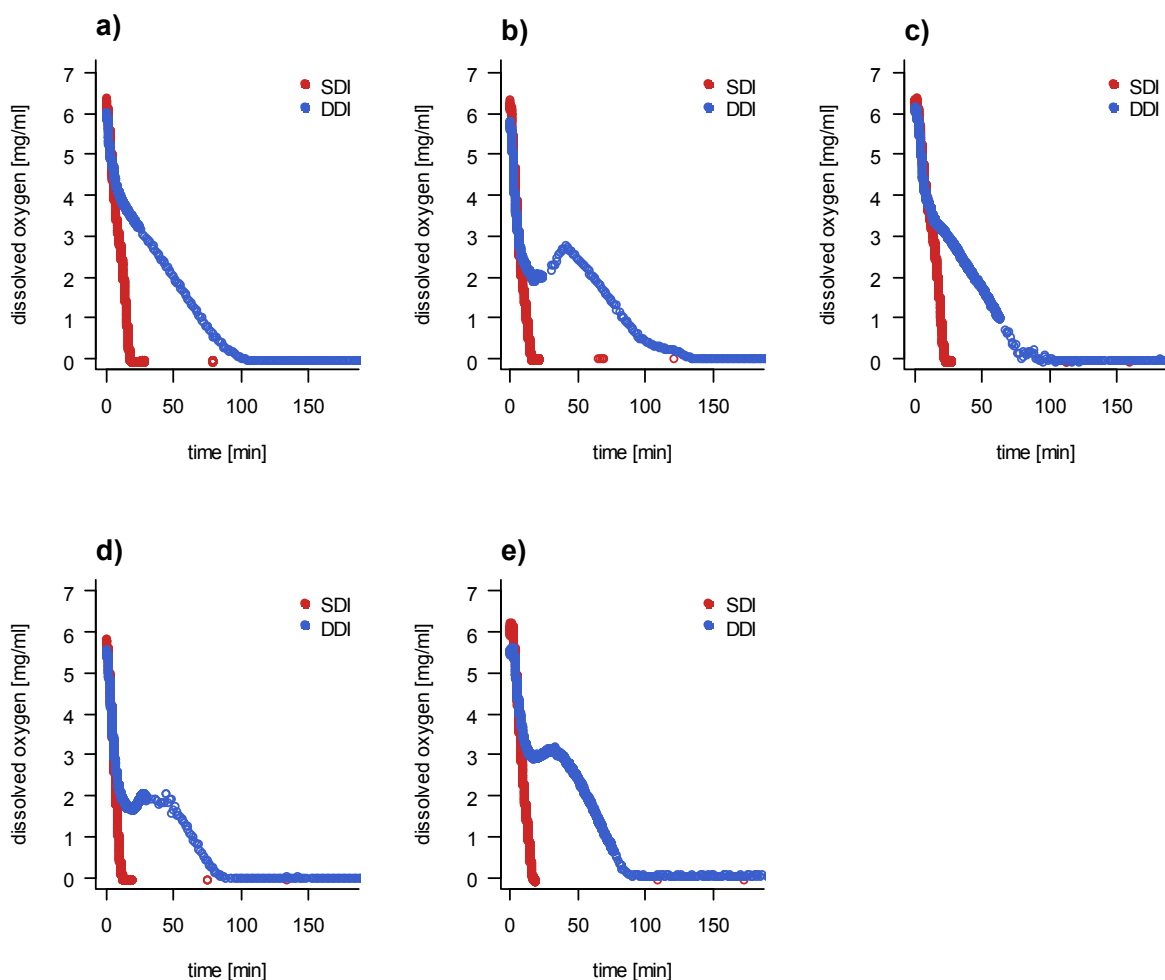


Fig. S3. Replicates for assessment of DDI impact on oxygen transfer rates. After ~ 40 min of dynamic droplet incubation the oxygen concentration eventually exhibited a ‘shoulder’ in its time course (b, d and e), reflecting biological variability amongst the replicates. Nevertheless, the time point of oxygen depletion was similar in all experiments (~ 100 min).

Droplet manipulation and analysis

Microfluidic operation

The fabrication of microfluidic chips is described elsewhere.⁹ Novec HFE7500 (3M, Germany) with 0.5% Pico-Surf (Dolomite, UK) surfactant was used as continuous phase. For droplet generation and reinjection, fluids were actuated by a flow-rate-controlled MFCS-EZ pressure pump (Fluigent, France) and neMESYS syringe pumps (cetoni GmbH, Germany). All microfluidic devices were connected via PTFE-tubings (OD: 1/16", ID: 0.5 and 0.25 mm). Droplets were generated with a rate of ~ 1500 Hz and

with a volume of ~ 170 pL. Variations in volume were monitored by default and never exceeded a coefficient of variance of 1.5%.

Optical setup

An Axio Observer Z.1 inverted microscope (Carl Zeiss, Germany) was used for droplet observation. Fluorescent samples, *i.e.* droplet-confined *E. coli* cells producing mCherry, were excited with an HXP 120C fluorescent lamp (Carl Zeiss, Jena) through a 550/25 bandpass filter, and the emitted light was filtered with a 605/70 bandpass filter. For darkfield imaging, we applied a 10x objective without phase plate, combined with an annular ring of a 100x objective in the condenser. A PIKE F032-B camera (Allied Vision Technologies, Germany) was attached to the side port for droplet imaging, and a custom-made photodetector or an avalanche photodiode (Si APD S8664-30K, Hamamatsu, Japan) was attached to the front port for droplet detection or fluorescence analysis, respectively. Triggered imaging was realized by equally splitting the transmitted light between the two microscope ports holding the photodetector and the camera.

Volume determination

To monitor the influence of DDI on droplet volume and polydispersity, PBS-droplets were incubated either statically or dynamically at 28 °C for various time periods applying different oil flow rates as indicated in Fig. S4. Subsequently, droplets were reinjected into a microfluidic chip and imaged in groups at 40 droplets/s. A total number of $\sim 60,000$ droplets was recorded per reinjection. Automated droplet volume estimation was implemented in C++ using the open-source computer vision library OpenCV.¹⁰ **Preprocessing:** Each droplet image was converted into an 8-bit gray level image. Background subtraction was applied by first computing an average droplet-free image and then subtracting it from each image. Preprocessing was completed by image inversion and smoothing with a Gaussian filter of size 3x3 px and a standard deviation of $\sigma = 2$ px. **Segmentation:** For edge detection we computed derivatives of the discrete first and second order by applying the Sobel operator to the difference image. To obtain edges with a width of one pixel, we subtracted the image with the second order derivative from the image with the first order derivative. The resulting

image was binarized by applying a fixed threshold at intensity $I = 5$ and subsequent thickening of diagonal edges. To remove noise, foreground regions smaller than 10 pixels were deleted from the image. This process was followed by an edge joining algorithm that connects isolated edge segments at the distance of one pixel from each other. Finally, foreground regions smaller than 50 pixels were removed to reduce artifacts in the image, followed by a second round of edge joining by applying two iterations of a morphological dilation operation and two iterations of a morphological erosion operation. The resulting image was used to identify single droplets based on the circularity criterion that the standard deviation of the signature does not exceed 2 pixels. **Volume estimation:** The droplet volume was calculated using the equation

$$v = 2\pi \frac{h}{2} \left(r - \frac{h}{2}\right)^2 + \left(\pi \frac{h}{2}\right)^2 \left(r - \frac{h}{2} \left(1 - \frac{4}{3\pi}\right)\right)$$

for pancake-shaped droplets in a channel of height h and for droplets of radius $r > h$.¹¹

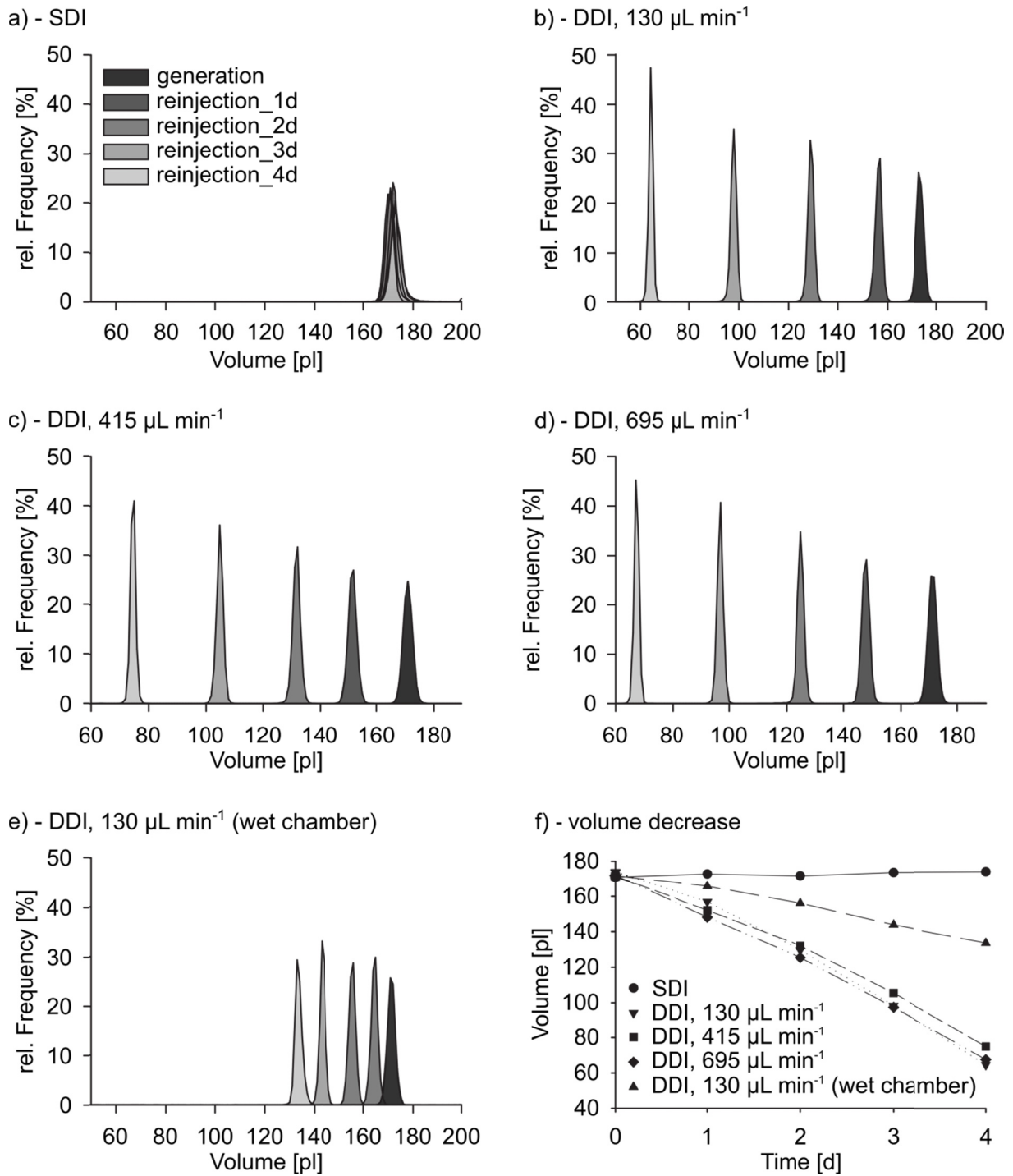


Fig. S4. Droplet volume change over prolonged times. Volume change was recorded over 5 days for SDI (a), and DDI at oil flow rates of 130 $\mu\text{L}/\text{min}$ (b), 415 $\mu\text{L}/\text{min}$ (c), and 695 $\mu\text{L}/\text{min}$ (e), respectively. The distribution width decreases over time, indicating that droplet polydispersity is maintained. This observation can possibly explained by increased evaporation rates in large droplets resulting from their larger surface area. The mean volume of droplets is decreasing with time. To minimize the decline in volume, the entire microfluidic setup was placed in a chamber with 100% relative humidity (e). Although droplet shrinkage could not be completely avoided, it was markedly reduced. f) Absolute means of volumes for all oil flow rates.

Determination of cell density

Triggered imaging of individual droplets was applied to determine the cell density of large droplet populations,⁹ recording 16-bit gray scale images. Image stacks were analyzed with Fiji, a distribution of ImageJ.¹² For image preprocessing, the averaged background was subtracted from each droplet image as described above and a median filter with the radius 1 was applied. Subsequently, the image was turned into a binary using the threshold method “Sauvola” with a radius of 15. Prior to droplet boundary detection with the “Analyze Particles” function, the “Fill Holes” and “Watershed” algorithms were applied to reduce the influence of cells on image segmentation. The region of interest was enlarged by -15 so that droplet boundaries were excluded and solely the inner droplet contributed to the mean gray value measured per droplet. In case of false image processing, respective images were manually excluded from further analysis.

For comparing the growth kinetics for different cultivation techniques (SDI, DDI, MTP and shaking flask) droplets were either reinjected from the incubator into a straight channel chip (SDI and DDI) or generated *de novo* from a shaking flask culture (Fig. S5). Since the limited volume of 96-well-plate cultures did not allow droplet generation for successive measurements, the cell density was measured at $\lambda = 620$ nm in a Fluostar Optima plate reader (BMG Labtech, Germany) and indirectly compared to droplet mean gray values by means of a calibration curve (Fig. S6).

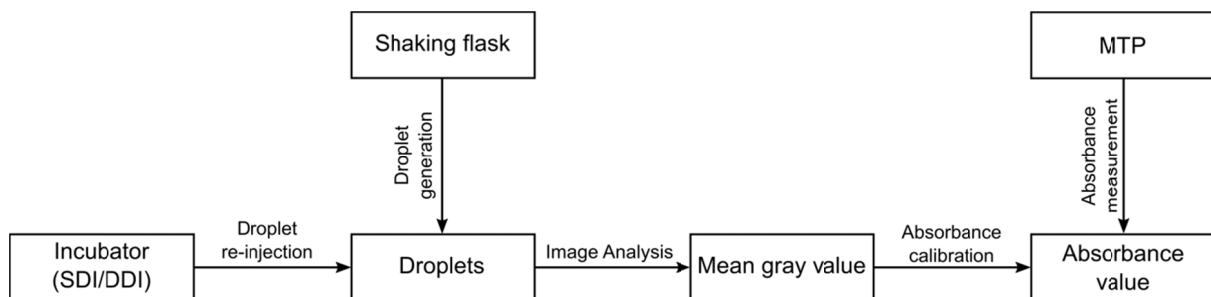


Fig. S5. Mean gray value determination for different cultivation methods.

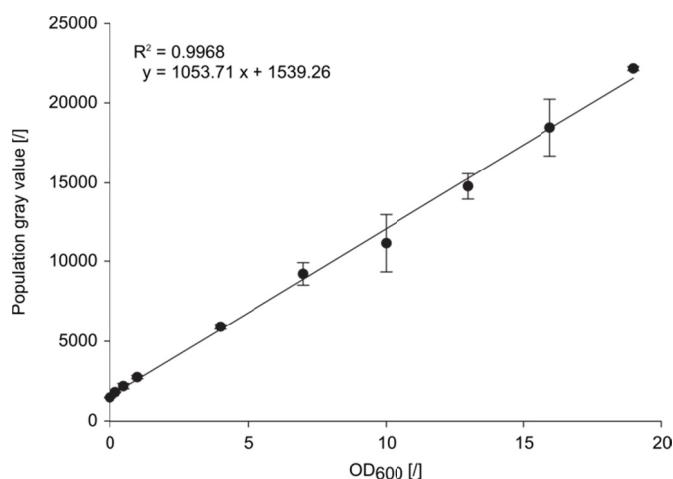


Fig. S6. Correlation between optical density measured at $\lambda = 600$ nm (OD_{600}) and population gray values (pgv). Cell suspensions adjusted to specific OD_{600} values were used to generate droplets. 2000 droplets were subsequently recorded with triggered imaging in darkfield illumination for each OD_{600} value. For the resulting 2000 droplet gray values a mean was calculated (= population gray value). Population gray values of three replicates are depicted here. Error bars indicate one standard deviation.

Fluorescence analysis

To directly compare the fluorescence intensity obtained with different cultivation methods, droplets were generated from shake flask as well as MTP cultures after 24 h of growth. Two detection techniques were employed to measure mCherry fluorescence intensities in droplets: In one approach, droplets were injected into a microfluidic chip and 16-bit gray scale images of grouped droplets in an observation chamber were recorded with a pco.edge 4.2 camera (PCO, Germany). In a second approach, the fluorescence intensity of sufficiently spaced droplets was monitored in a straight channel using an avalanche photodiode. The signal was logged by means of an USB-1608FS A/D converter (Measurement Computing, USA) and signal peaks were subsequently determined as a measure of droplet fluorescence.

Expression analysis of camelid antibody B10-6H

We analyzed the production of B10-6H,¹³ a VHH domain of a camelid antibody designed for amyloid detection, using western blots (Fig. S7). *E. coli* RV308 (p41-B10-6H) was grown for 18 h in MTP, shake flask and droplets as described above. To avoid protein misfolding and formation of inclusion bodies,

all cultures were incubated at 25 °C. Droplets were broken by adding 1H,1H,2H,2H-Perfluoro-1-octanol (Sigma, USA) at a 2:1 ratio to the emulsion. After 5 min incubation at RT and short centrifugation the aqueous phase was retrieved by pipetting. Irrespective of the cultivation method, cells were separated from culture medium by 5 min centrifugation at 16.000 *g*. Pellets were stored at -20 °C until further processing. For cell disruption, pellets were re-suspended in 15 µL of Bugbuster® Master Mix (Millipore, USA). After 20 min incubation at 30 °C with mild agitation, cells were subjected to 30 min ultrasonication. Proteins were denaturated by adding 6 µL NuPage® LDS sample buffer (Life Technologies, USA) and heating for 5 min at 95 °C. After blotting, the 6-histidine tag of B10-6H was detected with a specific monoclonal antibody Anti-His₆-Peroxidase (Roche, Switzerland) that is coupled to horseradish peroxidase. A Metal Enhanced DAB Substrate Kit (Thermo Fisher Scientific, USA) was used to detect the peroxidase. Band intensities were analyzed with the Fiji Gel Analyzer tool.

For blot A, the same sample volume (20 µL of cell suspension) was used for all cultivation approaches, allowing determination of recombinant protein concentration per volume unit. For blot B, samples were normalized by absorbance to account for the lower cell densities obtained with SDI and enable analysis of cell specific yields.

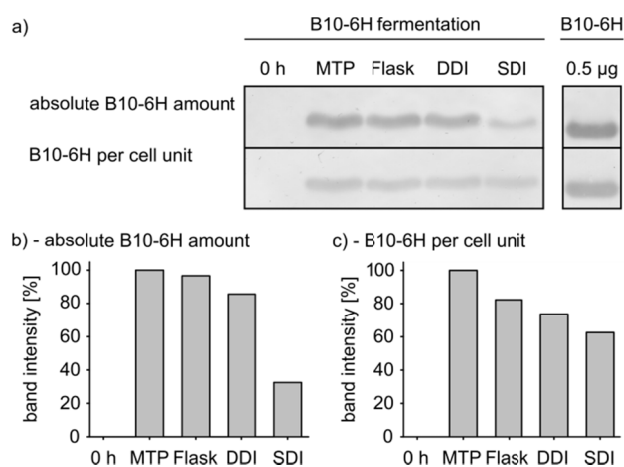


Fig. S7. Recombinant protein yield analysis (camelid antibody fragment B10-6H) for different cultivation methods. a) Western blots for volume-specific (A) and cell-specific (B) B10-6H yield analysis. b) and c) Band intensities from both plots

extracted with the image analysis software Fiji. Band intensities are standardized to the band intensity obtained from the MTP culture.

Remarkably, the protein concentration in a cell suspension derived from a pooled DDI droplet population reached the same range as the B10-6H concentration obtained in flask and MTP cultures (Fig. S7b). In contrast, only less than half of the B10-6H concentration was achieved with SDI (Fig. S7b) in consequence of hypoxic conditions and concomitant reduced cell densities. Yet, an observable reduction of the relative protein amount (standardized to cell density) indicates that the synthesis rate per cell is also affected (Fig. S7c).

Estimation of Oxygen Transfer Rates (OTR) during dynamic droplet incubation

To quantify OTR during DDI, we adapted the dynamic measurement method, which is frequently applied for stirred tank reactors. *E. coli* cells were encapsulated at OD 1 together with OXNANO sensors and incubated with continuous carrier oil recirculation, i.e. DDI. Subsequently, the oil circulation was halted (as in SDI) to estimate the *E. coli* OUR from the decrease in measured dissolved oxygen. After restarting the oil circulation, the rate of increase in measured dissolved oxygen plus the previously determined OUR results in the OTR of the system (Fig. S8). It is worth noting that residual oxygen dissolved in the oil phase may have lowered the measured OUR, negatively biasing the calculated OTR.

Interestingly, these experiments provide further evidence for the fast occurrence of inhomogeneous oxygen distribution among the droplet population. The initial peak observed after reactivating recirculation evidences that the droplets on the top and bottom borders of the emulsion exhibited higher dissolved oxygen concentrations (Fig. S8a).

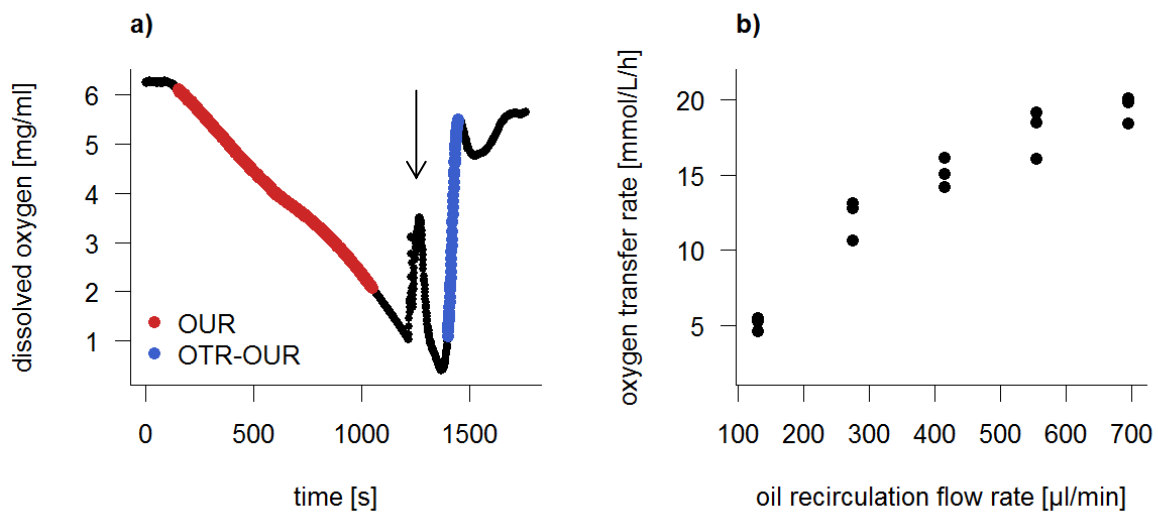


Fig. 58. Estimation of oxygen transfer rate by applying a dynamic gassing out method. a) Dissolved oxygen over time during dynamic gassing out with droplets containing respiring *E. coli* cells (oil recirculation speed: 275 $\mu\text{l}/\text{min}$). The red part of the graph was recorded after halting carrier oil recirculation. The slope of the decreasing DO was used to estimate the current OUR. After DO depletion the oil recirculation system was turned on leading to a sudden increase in DO (arrow) due to flushing droplets that had direct contact with perfluorinated oil at the bottom of the emulsion bulk through the measurement area of the incubator. During oil recirculation oxygen transfer is enhanced, resulting in an increase in DO (blue), which depends on OTR and OUR and is used to determine the OTR of the system. b) OTR estimates for five oil recirculation speeds.

Comparison of dynamic droplet incubation with emulsion shaking

1 ml of microfluidic emulsion, comprising 500 μl droplet bulk and 500 μl oil, were generated into multiple 2 mL reaction tubes with perforated lid (hole diameter: ~ 1 mm) and incubated in both humid saturated and non-humidified environments at 800 rpm (Thermomixer 5436, Eppendorf, Germany) and at 28 $^{\circ}\text{C}$. Such intermediate shaking frequency was selected since the shear of shaking did not influence droplet monodispersity within 24 h incubation in a pre-test. Moreover, this shaking frequency was used for *E. coli* cultivation in MTP and tubes, proving to be sufficient for oxygenation of the liquid culture.

Two different experiments were performed to characterize a) the stability of the shaken emulsions and b) the extent of oxygenation: For the first, PBS was employed as the aqueous phase, and the droplet size distributions were analyzed after 24 h and 96 h (Table S4). For the second, droplets containing *E. coli* were characterized after 24 h by measuring fluorescence levels (Fig. S11).

For a)

After 24 h, multiple large droplets were observed at the emulsion surface (Fig. S9). They are the result of emulsion failure and/or condensation on the tube walls. However, a large fraction of the analyzed droplets maintains its monodispersity, though showing considerably decreased volume due to evaporation (Table S4). Emulsion failure was drastic after 96 h, but by shaking inside a humidified environment this failure could be reduced even after 96 h (Fig. S10). Surprisingly, the strong decrease in average droplet volume could not be avoided by incubating in a humidified atmosphere.

Table S4. Average droplet volumes of emulsions incubated four days in agitated reaction tubes. The volume of min. 50,000 droplets was determined as described in the volume determination section. Averages and coefficient of variation (CV) are displayed for emulsions during generation and after one and four days of incubation. Very small (<50 pL) and very large (>300 pL) droplets are not reliably detected by the volume detection algorithm, therefore the CV of highly polydisperse emulsions, as is the case for the emulsion agitated with 800 rpm w/o humidification after 96 h, might be underestimated.

Emulsion Incubation	0 h		24 h		96 h	
Perforated tube, 0 rpm	170.5	1.4 %	146.4	7.9 %	125.6	25.0 %
Perforated tube, 800 rpm	171.7	0.9 %	121.6	7.9 %	95.7	22.7 %
Perforated tube, 0 rpm, humid	179.4	5.1 %	157.5	5.2 %	169.5	8.5 %
Perforated tube, 800 rpm, humid	176.3	1.6 %	120.9	6.3 %	105.0	10.8 %

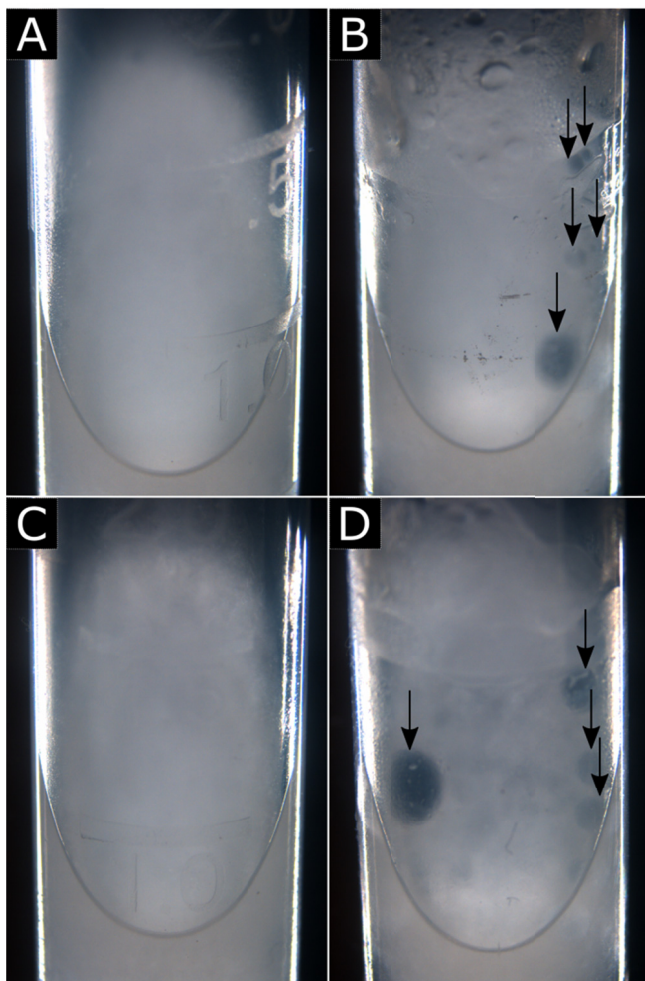


Fig. S9. Images of reaction tubes with PBS-droplet populations after 24 h of incubation. A – perforated tube, 0 rpm, B – perforated tube, 800 rpm, C – perforated tube, 0 rpm, humid, D – perforated tube, 800 rpm, humid. The arrows indicate visible large droplets that accumulated at the surface of the agitated emulsions.

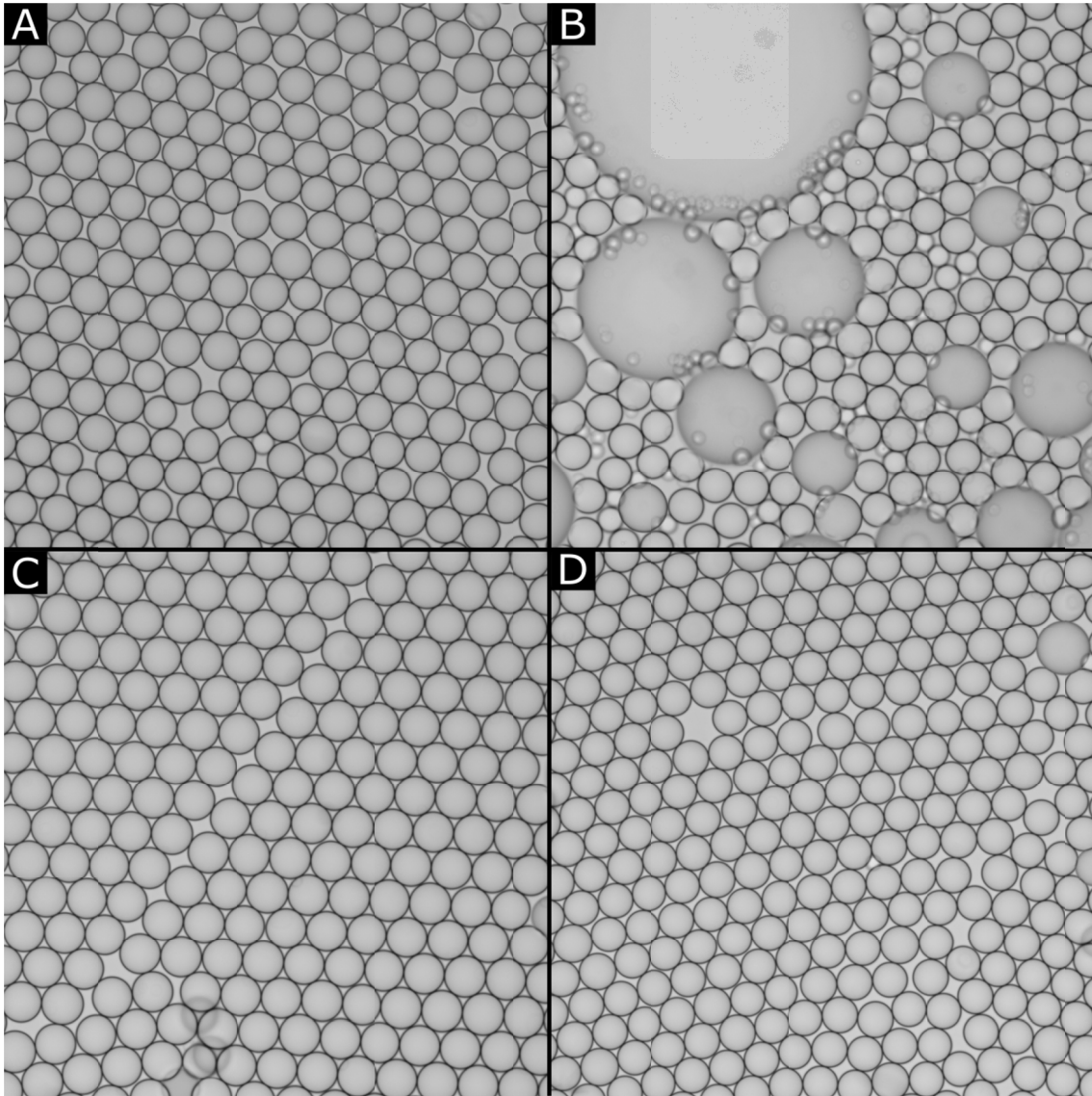


Fig. S10. Microscopic images of PBS-droplets after 96 h of incubation in agitated reaction tubes. A – perforated tube, 0 rpm, B – perforated tube, 800 rpm, C – perforated tube, 0 rpm, humid, D – perforated tube, 800 rpm, humid. Due to enhanced evaporation, the droplet polydispersity is markedly increased in the static tube, which was not observed to such extent when the static tube was placed in a humid chamber. While drastic emulsion failure was observed in the perforated tube at 800 rpm, the emulsion stability could be maintained when shaking the perforated tube in a humidified environment.

For b)

Shaking the emulsion in reaction tubes provides sufficient oxygen to increase cell growth and fluorescent protein production (Fig. S11). However, it is mandatory to perforate the lid of the reaction tube for aeration.

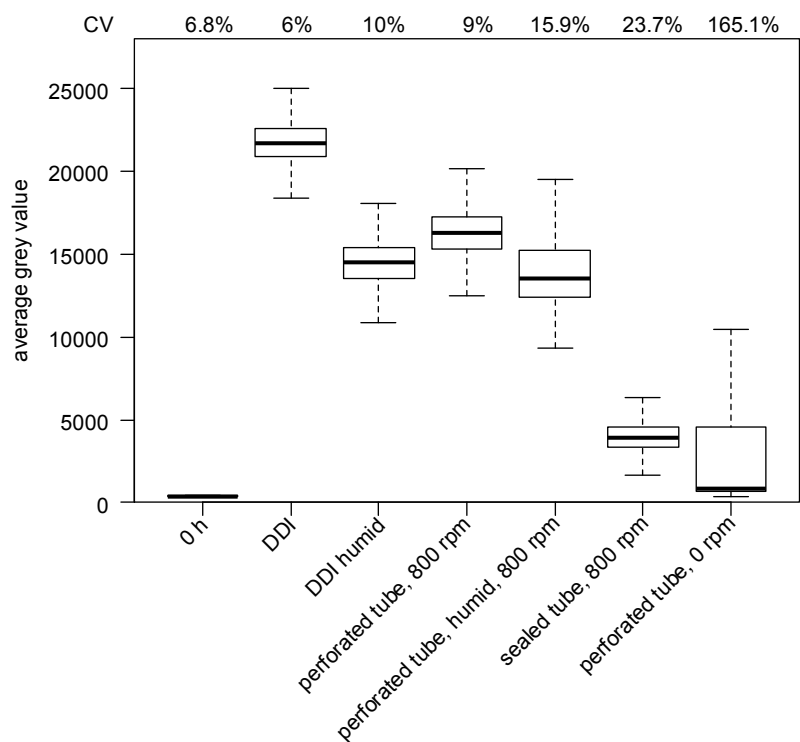
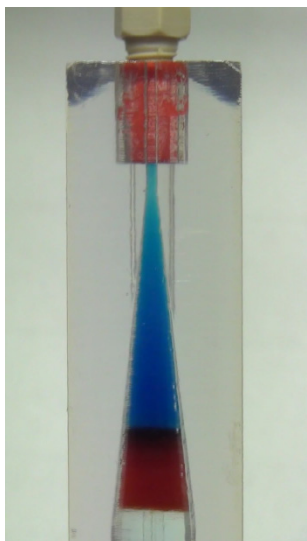


Fig. S11. mCherry fluorescence intensity of droplets incubated for 24 h in agitated reaction tubes or in DDI setup. Fluorescence intensities of at least 5000 droplets per incubation approach were derived from black and white images taken under fluorescence excitation. The bold line represents the median, while the upper and lower end of the box show the upper and lower quartiles. The whiskers extend to the furthest data point within 1.5 box lengths. Outliers are not shown.

Movie S1



Movie S1. Sequence of dynamic droplet incubation in the incubation device with colored droplets. Approximately 1.5 million blue droplets (0.25 mg/mL methyl blue in water) and 1.5 million red droplets (8.1 mg/mL phenol red in water) were directed to an incubator, which was connected to the DDI setup. The 10-fold faster time lapse video displays the droplet movement during the start of the oil recirculation at a flow rate of 130 $\mu\text{L}/\text{min}$. After ~ 15 min of oil recirculation the blue and red droplets are mixed homogeneously.

References

- 1 W. Salser, in *Genetic engineering*, ed. A. M. Chakrabarty, CRC, Boca Raton, Florida, 1979, pp.53-81.
- 2 M. Okanishi and K. F. Gregory, *J. Bacteriol.*, 1970, 104, 1086-1094.
- 3 T. Baba, T. Bae, O. Schneewind, F. Takeuchi and K. Hiramatsu, *J Bacteriol.*, 2008, 190, 300-310.
- 4 P. Joseph, J. R. Fantino, M. L. Herbaud and F. Denizot, *FEMS Microbiol. Lett.*, 2001, 205, 91-97.
- 5 M. Heldal, S. Norland and O. Tুমyr, *Appl. Environ. Microbiol.*, 1985, 50, 1251-1257.
- 6 P. Çalik, P. Yilgör, P. Ayhan, A. S. Demir, *Chem. Eng. Sci.*, 2004, 59, 5075-5083.
- 7 T. Beneyton, F. Coldren, J. C. Baret, A. D. Griffiths and V. Taly, *Analyst*, 2014, 139, 3314-3323.
- 8 J. Demas, B. Degraff and W. Xu, *Anal. Chem.*, 1995, 67, 1377.
- 9 E. Zang, S. Brandes, M. Tovar, K. Martin, F. Mech, P. Horbert, T. Henkel, M. T. Figge and M. Roth, *Lab Chip*, 2013, 13, 3707-3713.
- 10 G. Bradski, *Doctor Dobbs Journal*, 2000, 25, 120-126.
- 11 L. Boitard, D. Cottinet, N. Bremond, J. Baudry and J. Bibette, *Eng. Life Sci.*, 2015, 15, 318-326.
- 12 J. Schindelin, I. Arganda-Carreras, E. Frise, V. Kaynig, M. Longair, T. Pietzsch, S. Preibisch, C. Rueden, S. Saalfeld, B. Schmid, J. Y. Tinevez, D. J. White, V. Hartenstein, K. Eliceiri, P. Tomancak and A. Cardona, *Nat. Methods*, 2012, 9, 676-682.
- 13 G. Habicht, C. Haupt, R. P. Friedrich, P. Hortschansky, C. Sachse, J. Meinhardt, K. Wieligmann, G. P. Gellermann, M. Brodhun, J. Gotz, K. J. Halbhuber, C. Rocken, U. Horn and M. Fändrich, *Proc. Natl. Acad. Sci. U. S. A.*, 2007, 104, 19232-19237.